EPI International Journal of Engineering
Vol. 1, No. 1, February 2018, pp. 98-106
DOI: 10.25042/epi-ije.022018.15

ISSN:2615-5109

Deformation Analysis of Self-Expanding Stent Considering Plaque and a New Expanding Mechanism

Katsuhiko Sasaki,[a]* Yukiko Tomooka,[b] Ryo Takeda,[c] Achmad Syaifudin[d]

[a]Department of Mechanical Engineering, Faculty of Engineering, Hokkaido University. Email: katsu@eng.hokudai.ac.jp
[b]Department of Mechanical Engineering, Faculty of Engineering, Hokkaido University. Email: yukikotomooka@frontier.hokudai.ac.jp
[c]Department of Mechanical Engineering, Faculty of Engineering, Hokkaido University. Email: r.takeda@eng.hokudai.ac.jp
[d]Department of Mechanical Engineering, Institut Teknologi Sepuluh Nopember. Email: saifudin@me.its.ac.id

Abstract

In this research, effects of material properties of stent materials, such as nitinol and ferrous alloy, on a self-expanding stent are studied by the stent deployment simulations using finite element method (FEM). Stent, vessel, and plaque are modeled by using AutoCAD. The model is imported to a finite element analysis software Ansys 15.0 and the deployment analysis of the stent is carried out. In addition, two methods of the unsheathing of the self-expanding stent are studied: (1) a conventional method where a stent comes out from one end of the sheath and (2) a new method in which a stent comes out from the center of the sheath. Also, both the area stenosis ratio and Dog-Boning are discussed referring the simulations conducted in the paper.

Keywords: FEM; nonlinear deformation; plague; SMA; stent

1. Introduction

Recently, the number of deaths caused by the blood vessel related disease, such as heart diseases, is increasing in Japan. Atherosclerosis is one of the most serious and common form of vascular diseases [1]. A vascular stent is a small mesh tube used to open narrow or blocked arteries and restore blood flow. Stents are classified two types: one of them is a balloon-expanding stent and the other a self-expanding stent. The balloon-expanding stent uses the plastic deformation of the stent material caused by the balloon expansion, while the self-expanding stent uses the super-elastic deformation of the stent material such as the shape memory alloy. The self-expanding stents have an advantage to be able to recover even after complete flattening or radial crushing due to the pseudo-elasticity of shape-memory alloy (SMA). Thus, the self-expanding stents are suitable for superficial locations, such as the carotid and femoral arteries. On the other hand, the self-expanding stents represent the lower radial expansion force and are largely affected by the recoil force of artery than the balloon-expanding stents [2, 3].

*Corresponding author. Tel.: +81-(0)11-706-6414
Kita 13, Nishi 8, Kita-ku
Sapporo, Hokkaido, Japan, 060-8628

As for the balloon-expanding stents, there are some studies indicating that the balloon expanding stents use the high strength material which gives important advantages to them. For example, the cobalt-based alloy, which has the higher strength than stainless steels, allows thinner struts to maintain the radial strength [4]. The thin-strut stents tend to have the smaller radius than the thick-strut stents, therefore the high strength material makes it easier to reach distally [4]. In addition, recent clinical reports suggest that strut thinness may affect the restenosis rates [5-7]. Kastrati and Pache et.al demonstrated that the implantation of the thin-strut stents is associated with a significant reduction of the risk for restenosis compared with the thick-strut stents implantation [6, 7].

So far, Ni-Ti alloy has been widely used for the self-expanding stent materials. Recently, a high strength ferrous polycrystalline shape-memory alloys (SMA), which have superelastic strain range of more than 13%, have been developed [8]. However, the effects of these advanced materials, which have the higher strength and the extremely high superelasticity, on both the stent functions and stenting have not been verified yet. Finite element method (FEM) has an advantage to investigate the mechanical behavior of stenting. Since inappropriate stenting (e.g., overexpansion and insufficient expansion) results in the undesirable clinical events such as neointimal hyperplasia, restenosis,

thrombosis, and so on, it is important to understand the mechanical behavior of the stenting [9]. There have been some FEM analyses simulating the self-expanding stent placement into stenosed artery [10, 11].

Delivery systems for the self-expanding stents consist of a series of sheaths, catheters and guidewires. The self-expanding stents are manufactured in the expanded shape and then compressed and restrained in a delivery system [12]. Haller et al. suggested the importance of delivery technique in determining vessel wall apposition of the Enterprise self-expanding intracranial stent [13]. However, few analyses concerning the effect of delivery systems, especially unsheathing methods, of self-expanding stents on stent deployments have been conducted.

In this paper, the effect of material properties of the stent materials (i.e., nitinol and ferrous alloy) on the stenting was studied by stent deployment simulations using FEM. Stent, vessel, and plaque were modeled by using AutoCAD. The model was imported to a finite element analysis software Ansys 15.0. In addition, two methods of the unsheathing were studied: (1) the conventional method where a stent comes out from one end of the sheath and (2) a new method in which a stent comes out from the center of the sheath.

2. Analysis Method

2.1. Stent Geometry, FEM Model, and Delivery System

In this analysis, simulations of the self-expanding stent implantation to carotid artery with concentric plaque were carried out. Two kinds of stent materials and delivery systems were considered and the outcomes of the stent deployment were compared.

A stent, outer sheath, plaque and artery models were built by using AutoCAD and Inventor. Figure 1 shows the stent geometry used for this analysis. The stent model was generated as expanded state referring to the Palmaz stent released by Johnson and Johnson. The 3D stent model was generated by the following steps:

1) 2D geometry of the expanded state of stent was drawn by using AutoCAD.
2) 2D stent geometry was embossed to a cylinder and the cylinder was subtracted afterwards by using Inventor. FEM models used for this analysis are shown in Fig. 2.

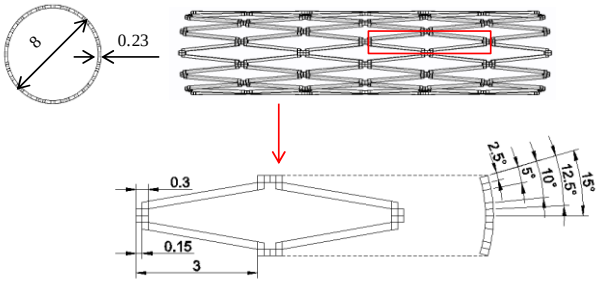

Figure 1. Stent geometry.

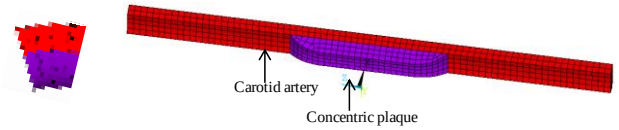

(a) Carotid artery and concentric plaque model

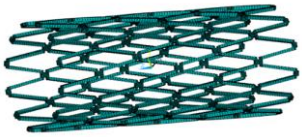

(b) Stent model at expanded state

Figure 2. FEM model

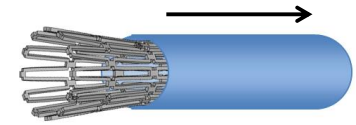

(a) Delivery system 1

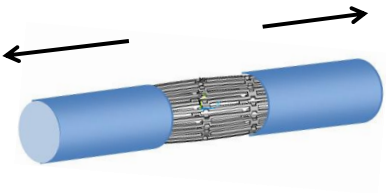

(b) Delivery system 2

Figure 3. FEM model

In this analysis, the plaque distribution was assumed to be concentric. Thus, the thickness of the plaque is constant in the circumferential direction. The plaque thickness is 1mm at the thickest part and the length 9.8mm, respectively. Artery was assumed to be a cylinder and the inner diameter, thickness, and length of the model are 6mm, 0.7mm, and 30mm, respectively. Since the unit cell of the stent is 30 degrees in the circumferential direction and the plaque distribution was assumed to be concentric, 30 degrees models in the circumferential direction were employed. An outer sheath was modeled as a rigid cylindrical surface, which has 19.8mm in length.

To consider the effects of the delivery systems, two methods of the unsheathing were studied as shown in Figs. 3(a) and 3(b): (1) the conventional method where a stent comes out from one end of the sheath and (2) a new method in which the stent comes out from the center of the sheath.

2.2. Material Properties

The material model used for the self-expanding stents was the super-elastic model available in Ansys 15.0. Figure 4 and Table 1 show the material parameters of the super-elastic materials. One of the most common self-expanding stents material Ni-Ti alloy and newly developed ferrous alloy, which has the higher strength and a larger super-elastic strain, were used for the stent materials. Table 2

summarizes the values of each parameter used in this analysis.

Mooney-Rivlin model given by Eq. (1) was used to demonstrate the hyper-elastic behavior of both the artery and plaque.

$$W = C_{10}(I_1 - 3) + C_{01}(I_2 - 3) + C_{20}(I_1 - 3)^2 + C_{11}(I_1 - 3)(I_2 - 3) + C_{30}(I_1 - 3)^3 \quad (1)$$

where I_1, I_2 and I_3 are the strain invariants, and C_{ij} are Mooney-Rivlin parameters. Mooney-Rivlin parameters used in this paper are shown in Table 3. Outer sheath was assumed to be a rigid surface model with negligible thickness.

Figure 5 shows the fitting of the stress strain curve of the ferrous alloy using the material parameters shown in Table 1. Fig. 6 shows the comparison of the stress strain curves of Ni-Ti with the ferrous alloys.

Figure 7 shows the stress strain curves of artery and plaques obtained by Mooney-Rivlin model with the material parameter shown in Table 3. Two types of plague were chosen: one is stronger than artery (Calcified plaque) and the other softer the artery (Cellular plaque).

2.3. Boundary Conditions

The cylindrical coordinate system was applied for the analysis conducted here. Therefore, *x* axis, *y* axis, and *z* axis show radial, circumferential, and longitudinal directions, respectively. Since 1/12 model in circumferential direction was used, both the circumferential ends of all the models were constrained in y direction. Moreover, both the longitudinal ends of vessel were constrained in all directions. Also, the stent models were restrained in z direction at the center. This analysis can be divided into 2 steps, the crimping process and the expansion process as shown in the below in details. To avoid rigid motion of both the vessel and the plaque, all the nodes of these models were constrained in the crimping process and the constraint was deleted in the expansion process.

Table 1. Stent material parameters [1, 10]

	σ_s^{AS} (MPa)	σ_f^{AS} (MPa)	σ_s^{SA} (MPa)	σ_f^{SA} (MPa)	ε_L	α
Ni-Ti	346	365	83	57	0.063	0.09
Ferrous alloy	719	941	265	113	0.175	0

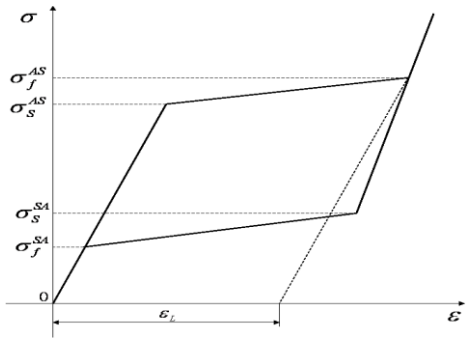

Figure 4. Material parameters for superelastic materials

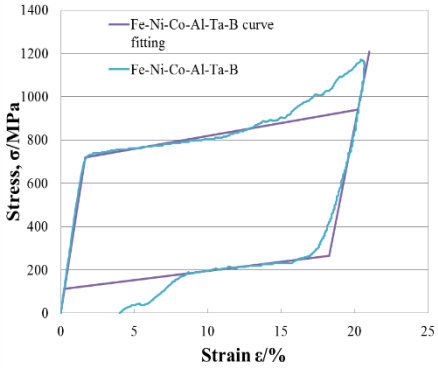

Figure 5. Stress-Strain curve fitting of the ferrous alloy

2.4. Contact Conditions, and Death and Birth of Elements

The contact definitions are important for the stent deployment analysis since the interactions of the stent with sheath or balloon and artery are one of the most important factors of the stenting process. Two surface-surface contact conditions are applied between the stent and sheath, and the vessel and stent, respectively. Between the stent and vessel, the node-surface contact was also defined since not only the stent's surface but also the stent's edge contact to the vessel wall.

Table 2. Stent material parameters [8, 10].

Component	Stent	Plaque	Vessel
Material	NI-Ti alloy Ferrous alloy	Calcified Cellular	Carotid
Yong's modulus [GPa]	60 43.8	2.19×10^{-3}	1.75×10^{-3}
Poison's ratio	0.33	0.495	0.495
Material model		Mooney Rivlin	Mooney Rivlin

Table 3. Mooney-Rivlin Parameters [15, 16].

	C_{10} [kPa]	C_{01} [kPa]	C_{11} [kPa]	C_{20} [kPa]	C_{30} [kPa]
Artery	18.9	2.75	85.7	590.4	0
Calcified	-496	506	1.19×10^3	3.64×10^3	4.74×10^3
Cellular	-803	832	1.15×10^3		

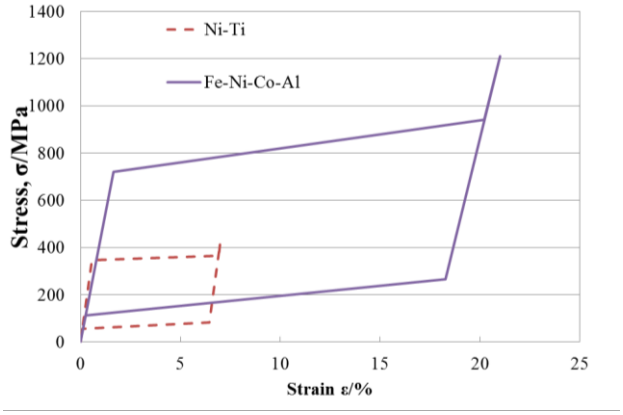

Figure 6. Stress-Strain curve of the stent materials.

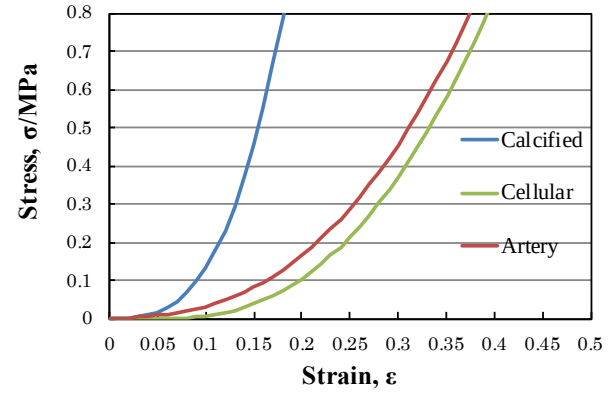

Figure 7. Stress-strain curve obtained from Mooney-Rivlin parameters.

In this analysis the "element birth and death" command was introduced to activate and deactivate the elements during the calculation. Since the diameter of self-expanding stents at the expanded state should be slightly larger than that of the vessel to open up and support artery wall, the diameter of vessel was modeled smaller than that of the stent in the beginning of the simulation. Thus, both the vessel and plaque models had to be deactivated to crimp the stent until its diameter reaches smaller than the vascular lumen diameter. Therefore, all the elements of both the plaque and vessel models were deactivated by using the element death command to prevent the contact of stent to both the vessel and plaque. In addition, the contacts between the stent and vessel or plaque do not occur in this process, then all the contact elements were also deactivated. In the stent expansion process, all the elements including the contact elements were activated by using the element birth command to consider the interactions of the stent with both the artery and plaque models.

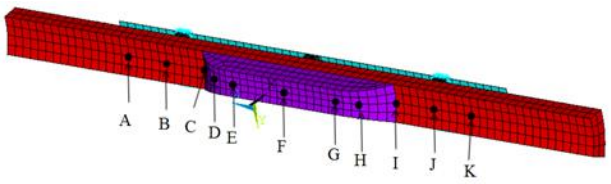

(a) Measuring points on the inner surface of the vessel wall

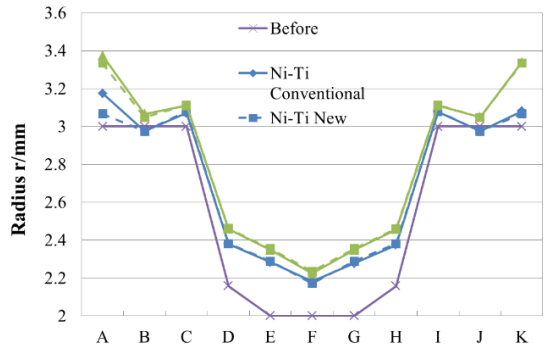

(b) Radii at each point on the vessel wall with calcified plaque after stent deployment

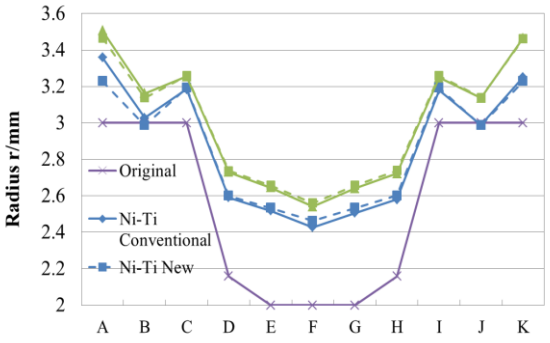

(c) Radii at each point on the vessel wall with cellular plaque after stent deployment

Figure 8. Radii of stent after expansion.

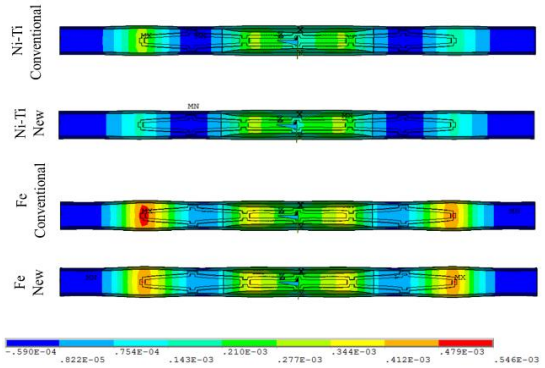

(a) Calcified plaque model

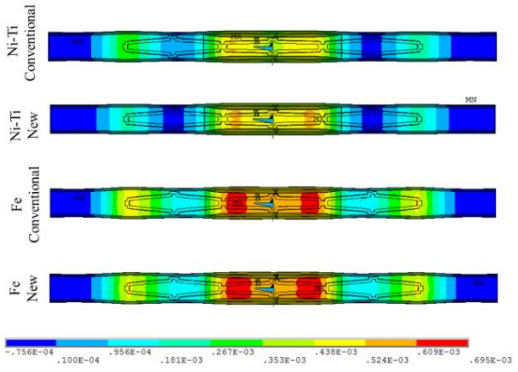

(b) Cellular plaque model

Figure 9. Radial displacement distribution after stent deployment.

3. Results and Discussions

3.1. Radial Displacement

Figure 8 shows the radii at each measuring point shown in Fig. 8(a) after the self-expanding stent placement. Fig. 8(b) shows the radius of the vessel wall with the calcified plaque after each stent deployment. Fig. 8(c) shows the radius of the vessel wall with cellular plaque after the stent deployment. The purple, blue, and green lines show the original radius, radius after Ni-Ti stent deployment, and radius after ferrous alloy stent deployment at each point on the vessel, respectively. The solid line shows the results using the conventional delivery system (delivery system 1), while the broken line the results using the new delivery system (delivery system 2). "Ni-Ti Conventional", "Ni-Ti New", "Fe Conventional" and "Fe New" on the figures in this section correspond to the results of "Ni-Ti alloy placement stent using the conventional delivery systems", "Ni-Ti alloy stent placement using the new delivery system", "Ferrous alloy placement stent using the conventional delivery systems" and "Ferrous alloy placement stent using the New delivery systems", respectively.

Figure 8(b) shows that the radius of the vessel becomes larger by using the ferrous alloy stent than using the Ni-Ti stent due to the higher strength of ferrous alloy though the differences were small. There is not large difference in the radius between the delivery systems except for the radius at measuring point A, where the stent and artery initially contact. In case of the conventional delivery system, the radius at the point A, where both the stent and vessel wall initially contacts, becomes larger than that at point K, where both the stent and vessel contact at the end of stent deployment process for both the stent materials. On the other hand, in case of using the new delivery system, the radius at both the point A and K become almost same values. In other words, the amount of expansion of the initial contact area becomes larger than that of the last contact area. Since the regions around the distal points of the stent (i.e. point A and K) are on the vessel wall without plaque, the expansion of stent did not become large, whereas enough expansion to restore blood flow is required around the plaque lesion. The stents have the "dog-bone effect" that both the distal and proximal ends of stents tend to expand largely compared to the center of stents. This can cause the vascular injury which leads to the in-stent neointimal formation and restenosis afterward. Therefore, the uniform expansion of stents is desirable to decrease a risk of the vascular injury. Some studies have conducted to find out an optimum stent geometry to reduce dog-bone effect [14]. The results shown in Fig. 8 indicate that using the new delivery system may help decrease excess expansion of distal part of stents.

Figure 8(c) also describes the similar results as Fig. 8(b). Comparing Fig. 8(c) with Fig. 8 (b), the radius become larger at all measuring points. This is because the soft plaque was displaced easily by the stent comparing with the hard plaque. In addition, the radius at the center of plaque (point F) becomes smaller by using the new delivery system than that by using the conventional delivery system though the differences were small. Larger difference of the radius between two delivery systems was observed in case of the Ni-Ti stent placement compared to the ferrous alloy stent placement.

In case of the conventional delivery system, the stent was released from one distal part to the other distal part (from measuring point A to K shown in Fig. 8(a)). Fig. 9 shows the radial displacement distribution after stent deployment: Fig. 9(a) the results of hard plaque (i.e. calcified plaque) model and Fig. 9(b) the results of soft plaque model (i.e. cellular plaque).

Figures 9(a) and 9(b) also clearly show that, when the conventional delivery system was used, the radial displacement of vessel wall, where both the stent and vessel wall initially contact, become larger than that of the other end, where both the stent and vessel wall lastly contact. The vessel wall near the plaque ends were not displaced largely, while the end of the stent expanded largely and displaced vessel wall. The ferrous alloy stent displaced larger than that of the Ni-Ti stent in all region of the vessel wall. Though the large expansion of the plaque is desirable, the ferrous alloy stents also displaced the vessel wall where the plaque does not exist largely. One of the reasons of the excess expansion at the end of the stent might be the stent geometry. By using other stent geometry which decreases the dog-bone effect with ferrous alloy stent, the larger expansion of the plaque lesion and the adequate expansion of the normal artery may be expected.

3.2. von Mises Stress

Figure 10(a) shows the von Mises stress on the stent after the stent placement to the hard plaque and Figure 10(b) that after the stent placement to the soft plaque. The maximal von Mises stress values induced on the stents are shown in Fig. 11. Figure 11(a) shows the calcified plaque and Figure 11(b) the cellular plaque, respectively.

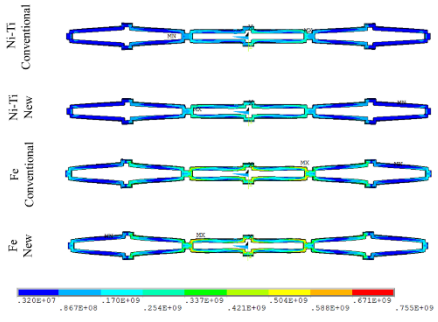

(a) Calcified plaque model

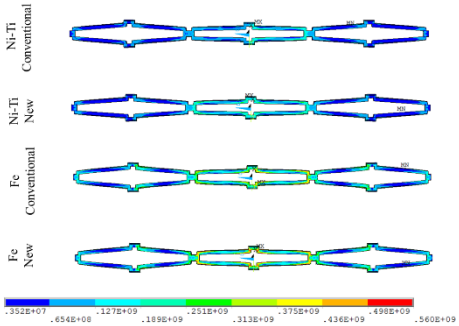

(b) Cellular plaque model

Figure 10. von Mises stress distribution

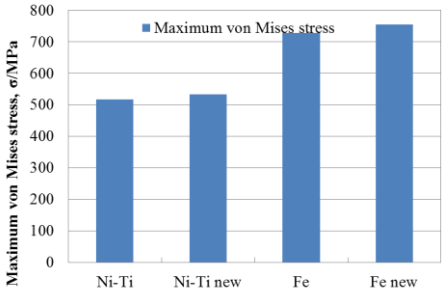

(a) Calcified plaque model

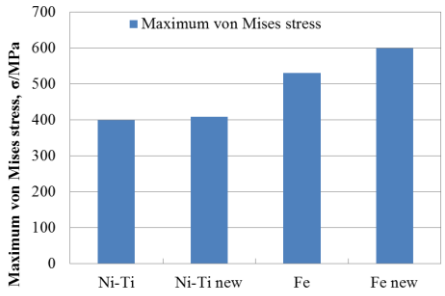

(b) Cellular plaque model

Figure 11. Maximum von Mises stress value induced on stents.

Figures 10 and 11 indicate that the higher von Mises stress was observed on the ferrous alloy stent than the Ni-Ti stent because of the different stress-strain relation of them. For all the delivery systems and stent materials, the stress concentrations were observed around the links of stents. The von Mises stress distributions on the stent were similar in all analyses.

The von Mises stress distributions on the plaque are shown in Fig. 12. Figure 12(a) shows the calcified plaque and Figure 12(b) the cellular plaque, respectively. The maximal values of the von Mises stress induced on the plaques are shown in Fig. 13. Fig. 12 shows that the von Mises stress value induced on the plaque becomes higher in case of the ferrous alloy stent deployment since the ferrous alloy stent has the higher strength and the larger self-expands than the Ni-Ti stent. The stress concentration was observed on the plaque where stent's circumferential edges contact plaque in the ferrous alloy stent deployment analyses. It is also found out from Fig. 13 that the stress values induced on the plaque were lower in the soft plaque than that of the hard plaque. The stress distributions of both the soft and hard plaque were similar.

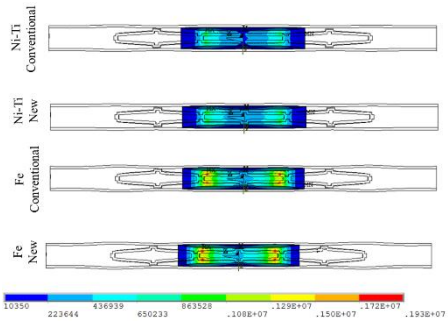

(a) Calcified plaque model

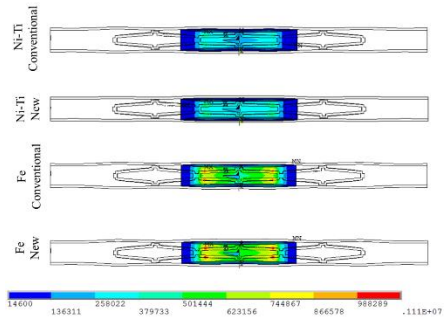

(b) Cellular plaque model

Figure 12. von Mises stress distribution

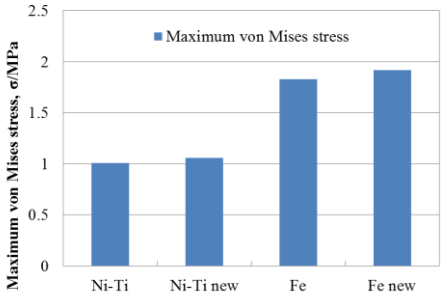

(a) Calcified plaque model

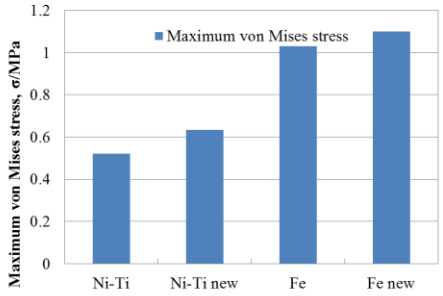

(b) Cellular plaque model

Figure 13. Maximum von Mises stress value induced on stents.

The von Mises stress distributions on the vessel wall are shown in Fig. 14. Figure 14(a) shows the calcified plaque

and Figure 14(b) the cellular plaque, respectively. The maximal von Mises stress values induced on the vessel walls are shown in Fig. 15. Figs. 14(a) and 14(b) show that the stress values induced on the vessel wall with the soft plaque was higher than that on the vessel wall with the hard plaque. From these results, it can be seen that the hard plaque absorbs the higher expanding load of the stent than the soft plaque. Therefore, the effect on the vessel wall with the hard plaque becomes lower. In addition, it can be found out that the stress concentrations on the distal ends of the vessel wall can be minimized by using the new delivery system. According to the results of the tensile tests of the human carotid artery, the initial failure begins around 0.2MPa and the ultimate failure occurs around 1.0MPa though the value varies from patients and clinical stages [17]. In this simulation, all the von Mises stress values induced on the vessel wall was lower than 0.2MPa. The highest value of 0.179MPa was observed by the ferrous alloy stent deployment with the conventional delivery system to the vessel with hard plaque. By using the new delivery system, the value decreased to 0.135MPa with keeping the amount of expansion of the plaque lesion. This indicates the effectiveness of using the new delivery system to reduce risks of the vascular injury by the stent deployments.

Figure 15(a) shows that maximal von Mises stress values induced on the vessel wall becomes smaller by using the new delivery system. However, the value was higher by using the new delivery system in case of the stent placement to the cellular plaque as shown in Fig. 15(b). This is due to the different location of the maximal von Mises stress. In case of the calcified plaque shown in Fig. 14(a), the maximal von Mises stress was induced on the end of the vessel wall because the hard plaque absorbed the higher stress. In case of the cellular plaque shown in Fig. 14(b), the maximal value was observed on the vessel wall under plaque. It is clarified that the larger stent expansion occurs at the initial contact area between the stent and vessel wall comparing with the area where the stent and vessel wall contact in the end. Therefore, the new delivery system has an advantage to reduce the stress at the end of the vessel.

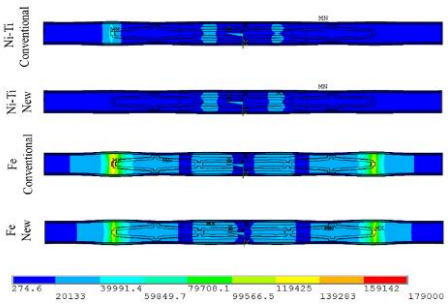

(a) Calcified plaque model

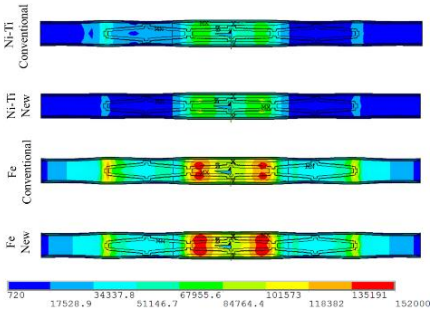

(b) Cellular plaque model

Figure 14. von Mises stress distribution on vessel wall after stent deployment

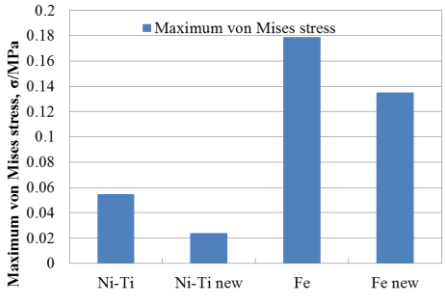

(a) Calcified plaque model

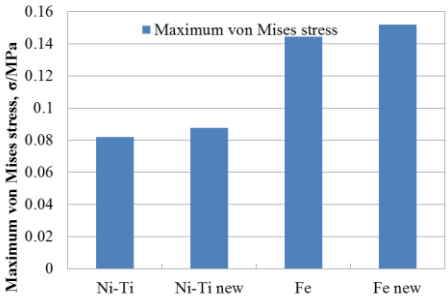

(b) Cellular plaque model

Figure 15. Maximum von Mises stress value induced on vessel walls

3.3. Area Stenosis Ratio and Dog-Boning

The area stenosis ratio is used to measure the severity of the stenosis. It is clinically used to measure the severity of narrowing of the blood vessel. Area stenosis ratio is defined by Eq. (2), where the cross-sectional area of the healthy blood vessel and that of the narrow blood vessel are denoted D and A, respectively. The area stenosis ratio changes are described in Fig. 16.

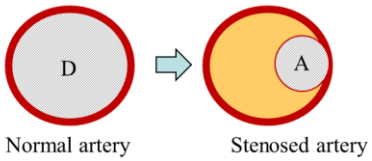

Figure 16. Definition of area stenosis ratio.

The stenosis ratio was calculated from the area of the narrowest part of the vessel (i.e. central cross-sectional areas of the lumen).

$$\text{Area stenosis ration} = (D\text{-}A)/D \times 100\ [\%] \quad (2)$$

The dog-boning is a phenomenon that the both stent's proximal and distal ends expand excessively like a dog bone shape. Though this phenomenon works to fix a stent to the vessel wall, ideally stent should be fixed to a vessel wall by pressure between full surface of stents and vessel wall [18]. In addition, the stent's edges with the dog-boning phenomenon becomes causes of the vascular injury which may lead to restenosis. Therefore, the dog-boning value should be minimized. The degree of the dog-boning can be defined by the Eq. (3).

$$\text{Dog-boning} = \frac{R_{POI}^{expanded} - R_{central}^{expanded}}{R_{central}^{load}} \quad (3)$$

where, $R_{POI}^{expanded}$ and $R_{central}^{expanded}$ are the radius at the point of interest (POI) and the central radius after the stent expansion, respectively. The dog-boning values were measured on the POI shown in Fig. 17. Dog-boning values on POI are summarized in the Tables 4(a) and (b). Table 4(a) shows the result of the calcified plaque model and Table 4(b) that of cellular plaque model.

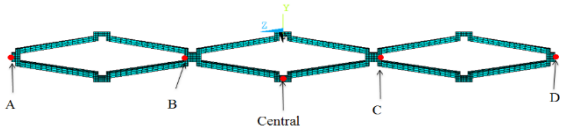

Figure 17. Points of interest

Table 4. Dog-boning on each measuring point
(a) Calcified plaque model.

POI	Ni-Ti [%]	Ni-Ti new [%]	Fe [%]	Fe new [%]
A	53.6	44.8	59.8	57.0
B	9.05	7.46	11.6	11.2
C	8.24	7.45	11.6	11.2
D	47.4	44.8	58.0	57.0

(b) Cellular plaque model.

POI	Ni-Ti [%]	Ni-Ti new[%]	Fe [%]	Fe new [%]
A	39.4	31.9	38.8	36.0
B	7.47	5.82	8.52	7.91
C	6.58	5.82	8.23	7.93
D	34.9	31.9	37.2	35.9

Figure 18 shows the relationship between the area stenosis ratio and the stent types. It can be seen that the area stenosis ratio becomes smaller by using the ferrous alloy stent than the Ni-Ti alloy stent. The area stenosis ratio becomes the smallest by placing the ferrous alloy stent with the new delivery system. The new delivery system has an advantage to reduce the area stenosis ratio compared with the conventional delivery system. This is because the new delivery system allows the larger expansion at the center of the stent, while the distal and proximal expansion are relatively larger by using the conventional delivery system. Similar tendency was observed in both the calcified plaque model and the cellular plaque model.

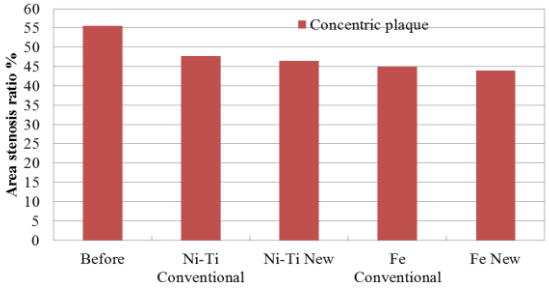

(a) Calcified plaque model

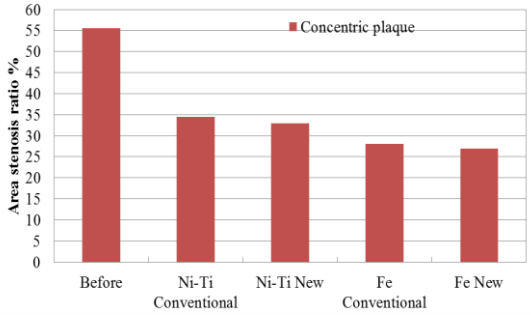

(b) Cellular plaque model

Figure 18. Area stenosis ratio after stent deployment

Some guidelines for the carotid artery stenting indicate that about 80% of the reference diameter is the recommended amount of expansion by stent. Reference diameter is measured at the internal carotid artery in the distal side of the plaque lesion in practice. In case of this analysis, the blood vessel was assumed to be a cylinder thus the diameter is constant. When the reference diameter is simplified as the diameter of the cylindrical blood vessel, approximately 36% of the area stenosis ratio would be the desired value after the stent expansion. The area stenosis ratio remained the high value even after the stent deployment in the calcified plaque model. On the other hand, the area stenosis ratio becomes acceptable level in case of the cellular plaque model. These differences between the calcified plaque model and the cellular place model were caused by their different stiffness. Since the calcified plaque is harder than the cellular plaque, the expansion by the stent was not enough in this analysis. In this analysis, the plaque and vessel wall were assumed to be mono layer though there are actually some layers and compositions. Therefore, using further detailed modeling of the plaque and vessel into analysis may improve the reality of the simulation.

Table 4 shows that the dog-boning values becomes lower by using the new delivery system compared with the conventional delivery system in both the stent materials (Ni-Ti alloy and ferrous alloy stents) and both the plaque compositions (calcified plaque and cellular plaque). In addition, the difference of the dog-boning values between the distal and proximal ends (POI A and D) was minimized

by using the new delivery system. These results show the effectiveness of the new delivery system on minimizing both the dog-boning values and the dog-boning value's difference between the distal and proximal ends. In the analysis using the calcified plaque model, the dog-boning values were higher with the ferrous alloy stent than that with the Ni-Ti alloy stent. This maybe because the ferrous alloy has the higher strength than the Ni-Ti alloy, therefore, the ferrous alloy stent expands largely on the vessel wall at the distal and proximal ends of the stent than the Ni-Ti stent. However, since the calcified plaque is harder than the vessel wall, the stent expansion might be restrained to a certain extent.

4. Conclusions

In this study, stenting using the two types of the stent materials (i.e. Ni-Ti alloy and ferrous alloy) and delivery systems are compared based on the simulations conducted by FEM analysis. As a result, the following conclusions were obtained.

(1) The ferrous alloy stent has the larger expansion than the Ni-Ti stent irrespective of the plaque distribution and composition.
(2) The ferrous alloy stent placement leads to the higher von Mises stress on the plaque and the vessel wall.
(3) The ferrous alloy stent increases the area stenosis ratio more than the Ni-Ti stent in both the concentric and the eccentric plaque analyses.
(4) The higher dog-boning value was observed in case of the ferrous alloy stent placement.
(5) The new delivery system has an advantage to reduce the excessive expansion at the distal and proximal ends of the stents.
(6) The new delivery system reduces the area stenosis ratio in all the results compared with the conventional delivery system.
(7) The new delivery system reduces the dog-boning value irrespective of the stent material, plaque composition, and plaque distribution.

References

[1] Ministry of Health, Labour and Welfare, Vital Statistic 2015.
[2] Duerig TW, Wholey M. A comparison of balloon- and self-expanding stents. Minim Invasive Ther Allied Technol 2002;11:173-178.
[3] Grenacher L, Rohde S, Gänger E, Deutsch J, Kauffmann GW, Richter GM. In vitro comparison of self-expanding versus balloon-expandable stents in a human ex vivo model. Cardiovasc. Intervent. Radiol 2006;29:249-254.
[4] Medtronic, Advantages of Cobalt Alloy for Coronary Stents 2003.
[5] Briguori C, Sarais C, Pagnotta P, Liistro F, Montorfano M, Chieffo A, Sgura F, Corvaja N, Albiero R, Stankovic G, Toutoutzas C, Bonizzoni E, Mario CD, Colombo A. In-stent restenosis in small coronary arteries: Impact of strut thickness. J. Am. Coll. Cardiol 2002;40:403-409.
[6] Kastrati A, Mehilli J, Dirschinger J, Dotzer F, Schühlen H, Neumann FJ, Fleckenstein M, Pfafferott C, Seyfarth M, Schömig A. Intracoronary stenting and angiographic results: strut thickness effect on restenosis outcome (ISAR-STEREO) trial. Circulation 2001;103:2816-2821.
[7] Pache J, Kastrati A, Mehilli J, Schühlen H, Dotzer F, Hausleiter J, Fleckenstein M, Neumann FJ, SattelbergerU, Schmitt C, Müller M, Dirschinger J, Schömig A. Intracoronary stenting and angiographic results: strut thickness effect on restenosis outcome (ISAR-STEREO-2) trial. J. Am. Coll. Cardiol 2003;41:1283-1288.
[8] Tanaka Y, Himuro Y, Kainuma R, Sutou Y, Omori T, Ishida K. Ferrous Polycrystalline Shape-Memory Alloy Showing Huge Superelasticity. Science 2010;327:1488-1490.
[9] Russo RJ, Silva PD, Yeager M. Coronary artery overexpansion increases neointimal hyperplasia after stent placement in a porcine model. Heart 2007;93:1609-1615.
[10] Wu W, Qi M, Liu XP, Yang DZ, Wang WQ. Delivery and release of nitinol stent in carotid artery and their interactions: A finite element analysis. J. Biomech 2007;40:3034-3040.
[11] Lally, C, Dolan F, and Prendergast PJ. Cardiovascular stent design and vessel stresses: a finite element analysis. J. Biomech 2005;38:1574-1581,.
[12] Stoeckel D, Bonsignore C, Duda S. A survey of stent designs. Minim. Invasive Ther. Allied Technol 2002;11:137-147.
[13] Heller RS, Malek AM. Delivery technique plays an important role in determining vessel wall apposition of the Enterprise self-expanding intracranial stent. J. NeuroInterventional Surg 2011;3:340-343.
[14] Lim D, Cho S, Park W, Kristensson A, Ko J, Alhassani ST, Kim H. Suggestion of Potential Stent Design Parameters to Reduce Restenosis Risk driven by Foreshortening or Dogboning due to Non-uniform Balloon-Stent Expansion. Ann. Biomed. Eng 2008;36:1118-29.
[15] Prendergast PJ, Lally C, Daly S, Reid AJ, Lee TC, Quinn D, Dolan F. Analysis of prolapse in cardiovascular stents: a constitutive equation for vascular tissue and finite-element modelling. J. Biomech. Eng 2003;125:692-699.
[16] Pericevic I, Lally C, Toner D, Kelly DJ. The influence of plaque composition on underlying arterial wall stress during stent expansion: the case for lesion-specific stents. Med. Eng. Phys 2009;31:428-433.
[17] Stemper BD, Yoganandan N, and Pintar FA. Methodology to study intimal failure mechanics in human internal carotid arteries. J. Biomech 2005;38:2491-2496.
[18] Yoshida S. Effect of Distal Stiffness against Dog-Boning. Comput. Mech. Conf 2014;2014:155-156.